THE IMPACT OF RECONSTRUCTION FILTERS ON ^{99M}TC MYOCARDIAL SPECT IMAGING

MUHAMMAD NUR SALIHIN BIN YUSOFF

UNIVERSITI SAINS MALAYSIA

2010

THE IMPACT OF RECONSTRUCTION FILTERS ON ^{99M}TC MYOCARDIAL SPECT IMAGING

by

MUHAMMAD NUR SALIHIN BIN YUSOFF

Thesis submitted in fulfilment of the requirements for the degree of Master of Science

Jun 2010

ACKNOWLEDGEMENTS

Above all, all praises to Allah SWT for giving me the strength and help to complete this thesis. I am indebted to many people who have assisted me in this research. I have been fortunate to have reaped the benefits of wisdom from my supervisor, Prof. Dr. Ahmad Zakaria. I am very grateful for his advice and guidance during my master study in School of Health Science, USM and in the completion of this thesis. I am also grateful to the staff of Department of Nuclear Medicine, Radiotherapy and Oncology, HUSM for their help and cooperation particularly to the radiographer, Mr. Khairul Nizam Jaafar for his assistance afforded to me in acquiring all the data images. I have appreciated, as well, the support from Ministry of Science, Technology and Innovation, Malaysia (MOSTI) via the Postgraduate Scheme throughout the period of my study. Special thanks are dedicated to my beloved wife, Nur Hartini Mohd Taib and our daughter and son, Nurul Iman and Muhammad Adib for their sacrifice, support and prayer for me. They have been and will always be my source of inspiration. I also thank my mother, Zawiah Mat Hussin, our family members, and my fellow friends for their prayer, encouragement and support. Finally, thank you to any individuals who have contributed in this research. May God repay your kindness.

TABLE OF CONTENTS

CHAPTER 5: RESULTS

CHAPTER 6: DISCUSSION

CHAPTER 7: CONCLUSION

LIST OF TABLES

LIST OF FIGURES

LIST OF ABBREVIATION

ANOVA	Analysis of variance
BTR	Background count to target count ratio
CAD	Coronary artery disease
ECG	Electrocardiogram
EDV	End diastolic volume
EF	Ejection fraction
ESV	End systolic volume
FBP	Filtered back-projection
FT	Fourier Transform
FWHM	Full width half maximum
LAO	Left anterior oblique
LEHR	Low energy high resolution
LHR	Lung-heart ratio
LPO	Left posterior oblique
LV	Left ventricle
QGS	Quantitative gated SPECT
RAO	Right anterior oblique
ROI	Region of interest
SD	Standard deviation
SNR	Signal-to-noise ratio
SPECT	Single photon emission computed tomography
SV	Stroke volume
T/B	Target-background concentration ratio
^{99m}Tc	Technetium-99m
^{201}Tl	Thallium-201

KESAN PENURAS PEMBINAAN SEMULA KE ATAS PENGIMEJAN PANCARAN FOTON TUNGGAL TOMOGRAFI BERKOMPUTER (SPECT) MIOKARDIUM MENGGUNAKAN ^{99M}TC

ABSTRAK

Kajian prospektif dan retrospektif ini dilakukan bagi menyiasat kesan penurasan ke atas kualiti imej dan parameter-parameter kefungsian dalam SPECT miokardium menggunakan pelbagai penuras pembinaan semula dan parameter-parameternya yang berkaitan. Dalam kajian kualiti imej (kajian prospektif), satu sistem fantom jantung (dengan kecacatan bersaiz 1.10 cm di dalam miokardium) dalam konsentrasi radioaktiviti ^{99m}Tc yang berbeza sebagai latar belakang telah digunakan dalam prosedur SPECT. Nisbah konsentrasi sasaran-latar belakang (T/B) 5.3, 4.0, 3.3, 2.7, 1.3, and 1.0 telah digunakan untuk mendapatkan imej-imej SPECT. Berdasarkan kajian SPECT, nisbah kadar bilang latar belakang kepada kadar bilang sasaran (BTR) bagi setiap T/B masing-masing ialah 0.2, 0.4, 0.6, 0.7, 0.8, dan 0.9 (T/B = 1.0 disingkirkan). Kualiti imej dianalisis berdasarkan kontras imej, nisbah isyarat-kepada-hingar (SNR), ketepatan saiz kecacatan, dan gred keseluruhan (timbang tara di antara kontras, SNR, dan ketepatan saiz kecacatan). Keputusan-keputusan menunjukkan, penuras-penuras yang berbeza menghasilkan nilai-nilai kontras, SNR, dan saiz kecacatan yang berbeza. Peningkatan dalam parameter frekuensi henti dan parameter tertib penuras telah meningkatkan kontras dan SNR, tetapi ketepatan saiz kecacatan berkurang. Penuras Butterworth mempunyai keupayaan untuk mengimbangi di antara kontras, SNR, dan ketepatan saiz kecacatan sementara penuras Gaussian pula bagus dalam penghasilan imej dengan kontras dan SNR yang tinggi. Kajian ini

mencadangkan supaya penuras Butterworth digunakan untuk menganalisis imej-imej SPECT sementara penuras Gaussian sebagai alternatif. Berdasarkan gred keseluruhan, parameter-parameter penuras Butterworth (0.40 Nq; n = 12), (0.45 Nq; n = 8), (0.75 Nq; n = 12), (0.80 Nq; n = 8), (0.80 Nq; n = 11), dan (0.80 Nq; n = 11) masing-masing didapati optimum bagi BTR = 0.2, 0.4, 0.6, 0.7, 0.8, dan 0.9. Bagi penuras Gaussian, parameter-parameter penuras (0.60 Nq; n = 10), (0.65 Nq; n = 12), (0.65 Nq; n = 14), (0.70 Nq; n = 14), (0.75 Nq; n = 14), dan (0.50 Nq; n = 20) masing-masing didapati optimum bagi BTR = 0.2, 0.4, 0.6, 0.7, 0.8, dan 0.9. Frekuensi henti optimum bagi penuras Butterworth dan penuras Gaussian menunjukkan perkaitan yang selanjar dengan BTR. Bagi penuras Butterworth, *Frekuensi henti = 0.227 + (0.715 × BTR);* R^2 *= 0.864,* $p < 0.01$ dan bagi penuras Gaussian, *Frekuensi henti = 0.538 + (0.236 × BTR);* $R^2 = 0.876$, $p < 0.05$. Dua persamaan ini telah digunakan untuk menjangkakan parameter-parameter kefungsian bagi empat pesakit yang menjalani SPECT miokardium menggunakan ^{99m}Tc berdasarkan nilai BTR setiap pesakit (kajian retrospektif berdasarkan data pesakit yang diambil pada tahun 2003). Isipadu diastolik akhir (EDV), isipadu sistolik akhir (ESV), isipadu strok (SV), dan pecahan keluaran (EF) telah dikira. Keputusan menunjukkan bahawa nilai-nilai EDV dan ESV bergantung kepada jenis-jenis penuras yang digunakan semasa proses pembinaan semula. Penuras Butterworth telah menghasilkan EDV dan ESV yang lebih rendah berbanding penuras Gaussian. Dicadangkan supaya hanya satu jenis penuras sahaja digunakan semasa proses pembinaan semula bagi memastikan interpretasi betul.

THE IMPACT OF RECONSTRUCTION FILTERS ON ^{99M}TC MYOCARDIAL SPECT IMAGING

ABSTRACT

This prospective and retrospective study was undertaken to investigate the effect of filtering on image quality and functional parameters in myocardial SPECT using various reconstruction filters and their associated parameters. In the image quality study (a prospective study), a cardiac phantom system (with 1.10 cm cold defect in myocardium) for different ^{99m}Tc radioactivity concentration as background was used in the SPECT procedure. The target-background concentration ratio (T/B) of 5.3, 4.0, 3.3, 2.7, 2.0, 1.3, and 1.0 were used to acquire SPECT images. Based on the SPECT studies, the calculated background count to target count ratio (BTR) for each T/B was 0.2, 0.4, 0.6, 0.7, 0.8, and 0.9 respectively (T/B = 1.0 was excluded). The image quality was analyzed based on image contrast, signal-to-noise ratio (SNR), defect size accuracy, and total grade (trade-off between contrast, SNR, and defect size accuracy). The results showed that, different filters produce different values of contrast, SNR, and defect size. The increase in cut off frequency and order of filter resulted in the increase in contrast and SNR, but the accuracy of defect size was reduced. Butterworth filter has the ability to balance between contrast, SNR, and defect size accuracy while Gaussian filter is good in producing image with high contrast and SNR. This study suggests that Butterworth filters can be used to analyze SPECT images while Gaussian filter can be an alternative. Based on total grade, the Butterworth filter parameters of (0.40 Nq; n = 12), (0.45 Nq; n = 8), (0.75 Nq; n = 12), (0.80 Nq; n = 8), (0.80 Nq; n = 11), and (0.80 Nq; n = 11) were found optimum for BTR = 0.2, 0.4, 0.6, 0.7, 0.8, and 0.9

respectively. For Gaussian filter, the filter parameters of (0.60 Nq; n = 10), (0.65 Nq; n = 12), (0.65 Nq; n = 14), (0.70 Nq; n = 14), (0.75 Nq; n = 14), and (0.50 Nq; n = 20) were found optimum respectively for BTR = 0.2, 0.4, 0.6, 0.7, 0.8, and 0.9. The optimum cut off frequency of Butterworth and Gaussian filters showed linear relationship with BTR. For Butterworth filter *Cut off frequency* = *0.227 + (0.715 × BTR);* $R^2 = 0.864, p < 0.01$, and for Gaussian filter *Cut off frequency = 0.538 + (0.236 × BTR);* $R^2 = 0.876, p < 0.05$. These two equations were used to predict the functional parameters of four patients who underwent ^{99m}Tc myocardial SPECT based on their BTR values (a retrospective study based on the patient data taken in 2003). End diastolic volume (EDV), end systolic volume (ESV), stroke volume (SV), and ejection fraction (EF) were calculated. The results showed that EDV and ESV values depend on the filter types applied during the reconstruction process. Butterworth filter produced lower EDV and ESV compared to Gaussian filter. It is recommended that only one filter type need to be used during reconstruction process to ensure correct interpretation.

CHAPTER 1

INTRODUCTION

1.1 Single Photon Emission Computed Tomography (SPECT)

Basically, single photon emission computed tomography (SPECT) is a radionuclide imaging which uses gamma ray emission as source of information. In SPECT, a computerized tomography imaging technique is utilized to reconstruct two-dimensional (2-D) images from multiple views or projections around the body to create a three-dimensional (3-D) image.

In principal, gamma camera of SPECT system consists of i) a lead collimator that limits the acceptance angle and define the spatial distribution of gamma radiation, ii) a scintillation crystal, normally sodium iodide doped with thallium (NaI(Tl)) that absorb the gamma photons and emit a faint flash of light, iii) an array of light sensitive photomultiplier tubes (PMT) that proportionately convert the distribution of scintillation light into electronic signal, iv) a position logic network that process electronic signal to output signal representing the x, y spatial position and energy of the individually detected gamma rays on an event-by-event basis, iv) a pulse height analyzer, v) a scaler-timer, and vi) a cathode ray tube (CRT) to display image (Zaidi and Hasegawa, 2006; Links and Graham, 1997). The basic principles and components of the SPECT gamma camera are shown in Figure 1.1.

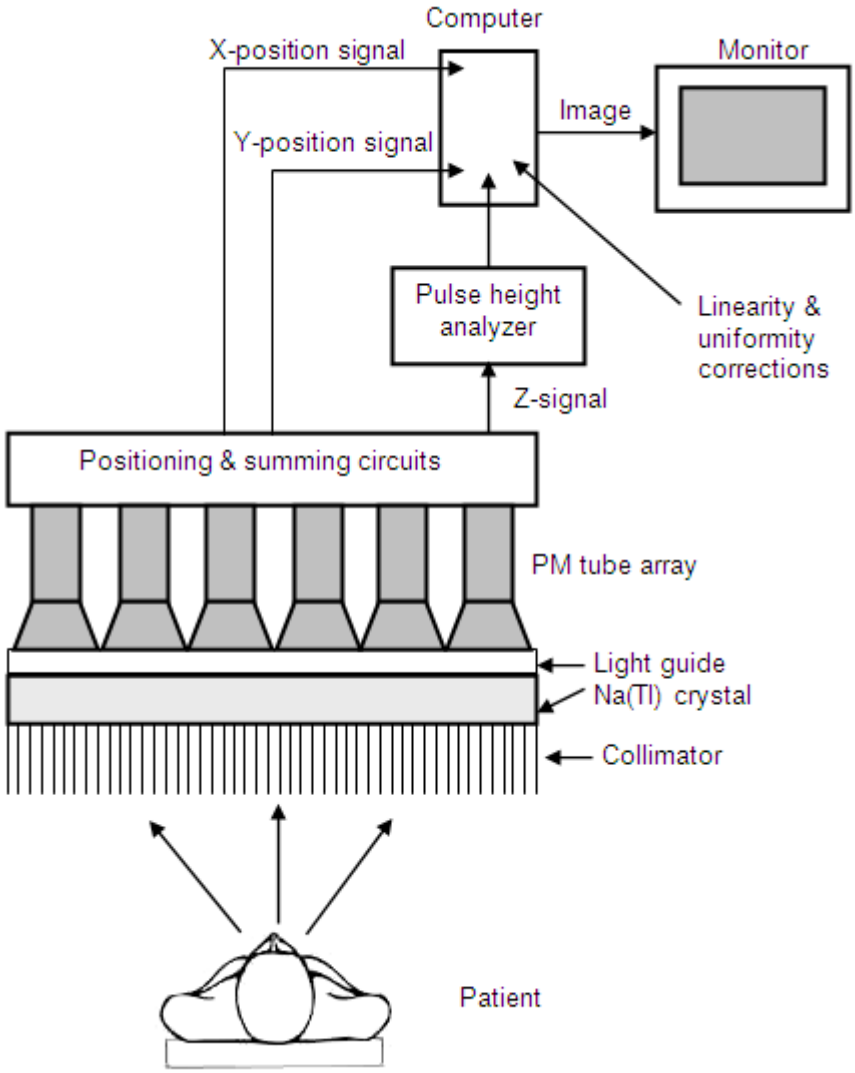

Figure 1.1 Basic principles and components of the SPECT gamma camera (Cherry *et al*., 2003).

1.2 SPECT Image Reconstruction

In nuclear medicine imaging, SPECT gamma camera rotates around the patient, taking pictures of radioisotope distribution within the patient from different angles. These two-dimensional (2-D) “pictures” are called *projections*, and the procedure to put the projections together to obtain a patient’s image in three-dimensional (3-D) is called *image reconstruction* (Zeng, 2001). The methods of image reconstruction from projection are also called methods of

tomographic reconstruction. *Tomography* has a Greek origin where *tomos* means slice and *graphy* means image or picture (Tsui and Frey, 2006). The concept of tomographic reconstruction from the projection images is pioneered by Bracewell and Riddle for astronomic applications in 1967 and extended to medical imaging by Shepp and Logan a few years later (Germano, 2001).

Many methods with different approach have been proposed for SPECT tomographic reconstruction either analytic algorithms such as filtered back-projection (FBP) or algebraic algorithms such as iterative reconstruction. However, FBP method remains the widely implemented and most understood and standardized (Cullom, 2001). Basically, FBP method involves several steps: i) acquiring data projection, ii) Fourier Transform (FT) of the data, iii) data filtering, iv) inverse Fourier Transform (FT) of the data, and v) back-projection of the filtered data (Cherry *et al.*, 2003; Tsui and Frey, 2006; Rusinek, 1995; Defrise, 2001; Defrise and Gullberg, 2006; Noo and Wagner, 2001; Zeng, 2001). One of the important tools in FBP method is reconstruction filter, purposely to smooth out the statistical noise. There are many types of SPECT reconstruction filters available such as Ramp, Butterworth, Gaussian, Hamming, Hanning, Parzen and others (Laere *et al.*, 2001). Refer to Chapter 2 for details of FBP method and SPECT reconstruction filters.

1.3 Radiopharmaceuticals

In nuclear medicine imaging for diagnosis of certain organs, one of the important things is perfusion agent called radiopharmaceutical. The important characteristics of radiopharmaceutical that want to used is it should be readily taken up by the target organ cells and should be retained at least for a

considerable length of time, to obtain sufficient information for reconstructing images. The physical properties of radiopharmaceutical used for imaging particularly their energy and bio-distribution in human body should also be safe and able to produce a quality of images.

There are several radiopharmaceuticals used in myocardial SPECT imaging, include ^{99m}Tc-based agents (^{99m}Tc-sestamibi, ^{99m}Tc-tetrofosmin, ^{99m}Tc-teboroxime and ^{99m}Tc-N-NOET) or Thallium-201 (^{201}Tl). Other radiopharmaceutical applied for cardiac SPECT studies are Iodine-123 in the form ^{123}I-methoxyiodobenzylguanidine (MIBG) to assess cardiac denervation, Indium-111 antimyosin to image necrotic myocardium from infarct or ischemic injury, and more recently fluorodeoxyglucose (^{18}FDG) at 511 keV with high-energy collimator for glucose utilization and viability (Cullom, 2001). However, the most widely used radiopharmaceuticals are Thallium-201 (^{201}Tl) and Technetium-99m (^{99m}Tc) due to their characteristics which suitable for myocardial studies (Case *et al*., 2004).

Thallium-201 (^{201}Tl), since the mid 1970s, has been clinically available and most popular radionuclide myocardial perfusion imaging for more than two decades. It is used particularly in detection and evaluation of patients with known or suspected coronary artery disease (CAD). It is a monovalent cationic radioisotope produced in cyclotron with half life $T_{1/2}$ = 73.1 hours. It decays by electron capture to mercury (^{201}Hg). In periodic table, ^{201}Tl is a metallic element in group IIIA, between potassium and rubidium. Due to its similarity to alkali metals such as caesium it penetrates through membrane cells and accumulates in cardiac and tumor cells. It has 68-80.3 keV (95% abundance) of x-ray emission, with photopeaks at 135.3 keV (2.7% abundance) and 167.4 keV

(10% abundance) of gamma emission (Taillefer, 2001; Corbett and McGhie, 1995; Strauss *et al*., 1997; Case, 2004).

However, there are some limitations of ^{201}Tl include their low energy for ideal SPECT imaging, and severely radiation dosimetry that limits injectable activity and image quality (Corbett and McGhie, 1995). In the late 1970s and early 1980s, many investigators tried to develop a new myocardial perfusion imaging agent labeled with ^{99m}Tc in order to overcome the limitations of ^{201}Tl (Taillefer, 2001). There are some advantages of ^{99m}Tc over ^{201}Tl, include extemporaneous reconstitution from a kit when required, more suitable photon energy (140 keV) which optimal for standard gamma camera imaging, resulting to better resolution due to less Compton scatter and less tissue attenuation in the patient (in comparison to the low energy of 68 to 80 keV for ^{201}Tl), much shorter half life (6.03 hours), and reduce patient radiation dosimetry permit for a higher injected activity (Higley *et al*., 1993; Rigo *et al*., 1994). With ^{99m}Tc, the simultaneously assessment of perfusion and function studies can be obtained in gated mode because of its better counting statistics (Taillefer, 2001).

1.4 Myocardial SPECT Perfusion and Function

Myocardial SPECT is a state of the art technique in nuclear medicine for the evaluation of myocardial perfusion and function within a single study. Myocardial perfusion allows evaluation of abnormality of radiotracer uptake by the heart muscle. While the myocardial function allows assessment of left ventricular (LV) function, either for regional such as wall motion and wall thickening, or global like volumes and ejection fraction (Berman *et al*., 2001; Hendel, 2004; Wackers, 2005). The ability to assess radionuclide myocardial

perfusion and function with gated SPECT imaging has revolutionized the field of nuclear cardiology.

Myocardial SPECT is undergoing significant changes in how it is used. When used conventionally, it produces radionuclide perfusion myocardial images, which are viewed qualitatively by radiologists, nuclear cardiologists or experienced physicians who work in nuclear medicine as three set of two dimensional images (short axis, vertical long axis and horizontal long axis), which contain about 15-30 slices each (Kurgan *et al*., 2001). Usually, this qualitative or visual analysis have two fundamental steps in process: identifying the pattern of count intensities in left ventricular (LV) myocardial images and comparing the pattern by using mental template for what constitute normal pattern (Folks, 2002; Kurgan *et al*., 2001).

The most recent method of myocardial SPECT imaging is by using ECG gating technique. Since its advent in 1990, physicians have found that the evaluation of myocardial perfusion and function are beneficial for diagnosis, risk stratification, and clinical decision making in their patients (Heller and Navare, 2004; Ficaro and Corbett, 2004). During the 1990s, by the availability of ^{99m}Tc perfusion tracers and advances in imaging hardware and software, gated myocardial SPECT became the standard image acquisition technique used in most nuclear medicine laboratories (Corbett and Ficaro, 2001).

The advantages of gated myocardial SPECT are its ability to quantitatively extract cardiac performance parameters as well as define and describe normality and abnormality criteria (Train *et al*., 2001; Lindahl *et al*., 1997). A wide range of cardiac parameters can be quantitatively measured (Germano *et al*., 1995; Germano *et al*., 1997; O'Connor *et al*., 2000; Rozanski

et al., 2000; Sharir *et al*., 2001; Slomka *et al*., 2005) and numerous published validation studies have shown their accuracy (Gunning *et al*., 1997; Yoshioka *et al*., 1999; Sharir *et al*., 2000; Bavelaar-Croon *et al*., 2000; Vallejo *et al*., 2000; Matsumoto *et al*., 2001; Itti *et al*., 2001; Nakajima *et al*., 2001; Nanasato *et al*., 2001) and reproducibility (Germano *et al*., 2000; Paeng *et al*., 2001; Akesson *et al*., 2004).

Besides providing incremental diagnostic and prognostic value compared to visual assessment alone (Germano, 2006), there are many advantages of quantitative measurements: lower price, shorter time, automatic recording of analysis results, consistency, and relatively inexpensive re-use of previous solutions (Kurgan *et al*., 2001). Acampa *et al*. (2000) in their study found that quantitative analysis has significantly higher sensitivity but lower specificity compared with visual analysis. Now, many guidelines have been discussed in order to achieve the high standard of qualitative and quantitative analysis (Strauss *et al*., 2002; Klocke *et al*., 2003; Douglas *et al*., 2006).

Basically, quantification of LV volumes involve the estimation of midmyocardium which corresponds to the maximal myocardial count, the process of detection the LV endocardial and epicardial boundaries either using fixed number of standard deviation (SD) of Gaussian fitting to the myocardial count profile or using a predefined count threshold based on the phantom data, and lastly calculation of the LV volumes: end diastolic volume (EDV), end systolic volume (ESV), stroke volume (SV), and ejection fraction (EF) (Paul and Nabi, 2004; Germano *et al*., 2001). The approaches of the quantification differ according to the nature of the quantitative algorithm used (Germano *et al*., 1995; Sharir *et al*., 2001). Now, there are many commercially software

programs available that provide automatic quantification such as Quantitative Gated SPECT (QGS), Emory Cardiac Toolbox (ECT), 4D-MSPECT, and Perfusion and Functional Analysis for Gated SPECT (pFAST) (Nakajima *et al*., 2001). Refer to Chapter 3 for details of LV volumes and EF quantification.

1.5 Issues in Myocardial SPECT Imaging

Although the quantification can be done automatically, the accuracy of the calculations are greatly affected by the quality of image obtained after the process of image reconstruction (Zaidi and Hasegawa, 2006). Filtered back projection (FBP) is the common and widely used method for image reconstruction process. In clinical practice, filter is used during FBP reconstruction process to reduce image noise, increase contrast and signal to noise ratio (SNR), and enhance the ability to detect any abnormalities in myocardial images. In principle, filter is a mathematical function that is applied to pixels in an image. Generally, the goal of filtering is to eliminate as much noise and retain as much signal as possible (Groch and Erwin, 2000). This includes smoothing, edge enhancement and resolution recovery. Most of filters are characterized by their cut off frequency and order parameters. The cut off frequency defines the frequency from which higher frequencies will be suppressed and therefore denotes the bandwidth of the filter. The amplitude of the filter at cut off frequency is dependent on the type of the filter. Some filters are defined by a second parameter, the order of the filter (e.g. Butterworth and Gaussian filters). The order tunes the filter by changing the slope of the filter function and allows the user to optimize the proportion smoothness–sharpness of the image (Laere *et al*., 2001).

In FBP process, the raw data must first be filtered by a function known as linear ramp filter in the spatial frequency domain. The ramp is necessary filter, as it removes the blurring effect or star artifact of the projection process. However, the application of ramp filter alone will result in extremely noisy images and unreadable for diagnostic interpretation. To overcome this problem, additional filter is applied to the projection data (Groch and Erwin, 2000; Laere *et al.*, 2001). The most commonly used additional filters are Butterworth, Gaussian, Hamming, Hanning, and Parzen. The Butterworth, Hamming, Hanning, and Parzen filters are low pass filters, while the Gaussian is a band pass filter (Rusinek, 1995; Madsen and Park, 1985). However, in FBP the combination of ramp filter and low pass filter could also function as a band pass filter (Susie, 2003). This combination reduces high frequencies, improves star artifacts, and provides a better image quality. The degree of smoothing is proportional to cut off frequency parameter, which can be expressed as a value either 0 to 1 Nyquist (Nq) range or 0 to 0.5 cycle/pixels range, depending on the particular convention adopted (Corbett and McGhie, 1995). Refer to Chapter 2 for details of SPECT reconstruction filters.

Usually, default additional filter and filter parameters are recommended by manufacturer for clinical use to avoid false results caused by over filtering. For example, in ADAC Forte SPECT imaging system, Butterworth filter at 0.55 cut off frequency and 5 order of filter are used as default for regular and gated SPECT imaging. However, in real practice, the application of filter and its parameters cannot be generalized in all situations. The choosing of filter and its parameters depend on several factors: the number of counts (limited by patient radiation burden and by increased movement artifacts related to study time), the

type of study (organ), the background of noise level, and the personal choice of the interpreting physician (Laere *et al*., 2001). There is no standard filter for universal application in clinical studies (Manrique *et al*., 2003) and only very limited literature exists on selection of appropriate filter parameters for practical purposes (Laere *et al*., 2001). The choosing of the appropriate filter, cut off frequency and order of filter is a matter of trial and error and depend on the specific radioisotope, protocol (Germano *et al*., 2001) and imaging system used (Mann, 2004). Inappropriate filtering of the raw back projected tomographic data may significantly degrade image quality and affect the accuracy of quantitative results (Vera *et al*., 1999; Wright *et al*., 2002; Vakhtangandze *et al*., 2005).

1.6 Literature Review

The determination of filter and its parameters need to be carried out so that the quantitative results of gated myocardial SPECT are accurate and valid for clinical practice (Gilland *et al.*, 1988). In determination the optimum filter parameters for myocardial SPECT, Takavar *et al*., (2004) used a phantom simulating heart left ventricle that was injected with 1 mCi (37 MBq) of ^{99m}Tc. Some balloons located inside the body phantom were filled with 1 mCi (37 MBq) of ^{99m}Tc as a body background. SPECT procedure was carried out and SPECT slices were reconstructed using Parzen, Hamming, Hanning, Butterworth, and Gaussian filters. They found that the cut off frequency of 0.3 Nq provided optimum defect size, 0.325 Nq indicated the best contrast, 0.5 Nq offered the best signal-to-noise ratio (SNR), and 0.325 gave the best overall result for Hamming filter. For Hanning filter, the cut off frequency of 0.3 Nq provided optimum defect size, 0.5 Nq indicated the best contrast, 0.45 Nq offered the

best SNR, and 0.5 Nq gave the best overall result. While for Butterworth filter, the cut off frequency of 0.3 Nq and order 8 provided optimum defect size, 0.6 Nq and order 8 indicated the best contrast, 0.45 Nq and order 11 offered the best SNR, and 0.45 Nq and order 11 gave the best overall result. For Gaussian filter, the cut off frequency of 0.5 Nq and order 10 provided optimum defect size, 0.6 Nq and order 20 indicated the best contrast, 0.4 Nq and order 22 offered the best SNR, and 0.5 Nq and order 20 gave the best overall result. The Parzen filter was visually excluded from their study because they could not even see the heart hole properly.

The relation between the optimum cut off frequency and the different amount of radiopharmaceutical administered has been studied by Ohnishi *et al*. (1997). They used a phantom injected with 2.2 MBq (0.06 mCi) and 10.6 MBq (0.3 mCi) ^{99m}Tc. The images were reconstructed using thirteen different cut off frequencies of Butterworth filter. Optimal cut off frequencies were determined by visual assessment and calculating normalized mean square error (n.m.s.e). They found that the optimal cut off frequencies for 2.2 MBq was lower than the optimal cut off frequencies for 10.6 MBq. From analysis, by using visual assessment, the cut off frequencies of 0.225 cycles/pixel (or 0.45 Nq) was found optimum for 2.2 MBq, while the cut off frequencies of 0.275 cycles/pixel (or 0.55 Nq) and 0.25 cycles/pixel (or 0.5 Nq) were found optimum for 10.6 MBq. On the other hand, by using n.m.s.e, the cut off frequencies of 0.225 cycles/pixel (0.45 Nq), and 0.275 cycles/pixel (0.55 Nq) were found optimum for 2.2 MBq and 10.6 MBq respectively.

Besides depending on the amount of radiopharmaceutical, there was also a study suggesting that the cut off frequency should be determined by

referring to the total counts. In this study, Minoshima *et al*., (1993) used Butterworth filter (0.07 to 0.18 cycle/pixel with 0.01 step) for a normal volunteer which underwent ^{99m}Tc brain SPECT imaging with five different acquisition times. The optimum cut off frequencies of Butterworth filter were determined by calculating normalized mean square error (n.m.s.e) on the reconstructed images. They found that the optimum cut off frequencies for individual cases can be reasonably estimated from a standard count-cut off frequency nomogram (Figure 1.2).

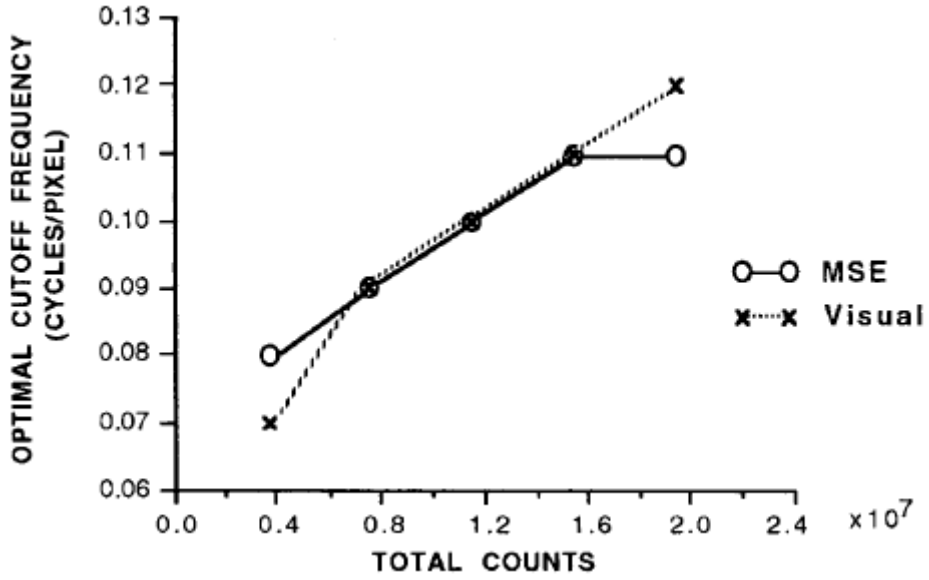

Figure 1.2 A nomogram describing relationship between total count and optimal cut off frequencies in brain SPECT. Optimal cut off frequencies determined by mean square errors (MSE) and visual inspection (Minoshima *et al*., 1993).

The effect of reconstruction filter on functional myocardial quantifications has been investigated by Vakhtangandze *et al*., (2005). They performed their study using ^{99m}Tc-Sestamibi gated myocardial perfusion SPECT image datasets from 30 patients reconstructed with cut off frequency 0.25 cycle/pixel (or 0.5 Nq) order 4 of Butterworth filter, and order 8, FWHM 4.0 mm of Metz filter. They

found that, with Metz filter rather than Butterworth filter, EDV and ESV were significantly larger, EF was significantly lower, and SV was not changed significantly. Spearman's rank correlation coefficients between results calculated with Metz and Butterworth filters were 0.96 for ESV, 0.88 for EDV, 0.94 for EF and 0.74 for SV.

According to Laere *et al.* (2001), for the purpose of clinical practice, the appropriate filter parameters obtained using certain type of imaging system cannot be directly extrapolated to other imaging system. However, it can be used as a general guideline. Therefore, the appropriate filter and its parameters for specific situation and imaging system need to be carried out.

1.7 Aims and Objectives

The aim of this research is to investigate the effect of filtering on image quality and functional parameters using various filter types and their associated parameters in ^{99m}Tc myocardial SPECT studies. The objectives of this research are:

i. To examine the effect of Butterworth, Gaussian, Hamming, Hanning, and Parzen filters and their parameters (cut off frequency and order) on the image quality.
ii. To determine the optimum filter and parameters for myocardial SPECT studies.
iii. To investigate the relation between the optimum cut off frequency for each filter and background count to target count ratio (BTR) obtained in SPECT images for clinical application.

CHAPTER 2

SPECT IMAGE RECONSTRUCTION: FILTERED BACK-PROJECTION METHOD

2.1 Principles of Filtered Back-Projection (FBP)

Filtered back-projection (FBP) is an analytic reconstruction method which involves several steps: a) acquiring data projection, b) Fourier Transform (FT) of the data, c) data filtering, d) inverse FT of the data, and e) back-projection of the filtered data, as graphically summarized in Figure 2.1 (Cherry *et al.*, 2003; Tsui and Frey, 2006; Rusinek, 1995; Defrise, 2001; Defrise and Gullberg, 2006; Noo and Wagner, 2001; Zeng, 2001).

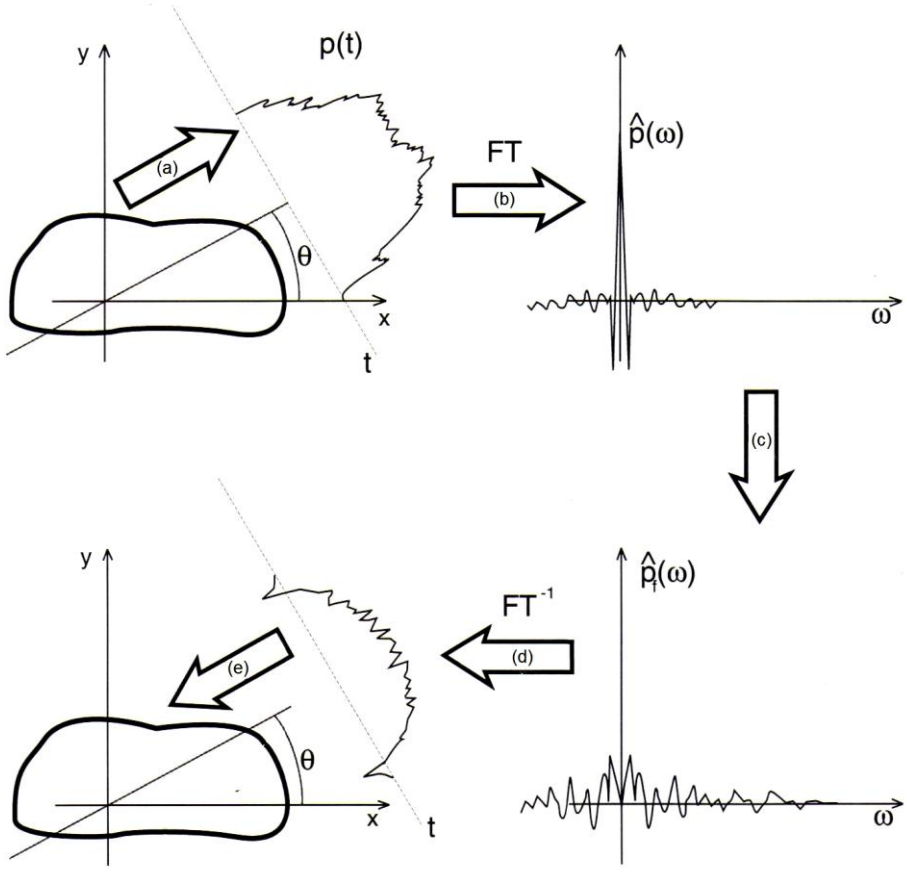

Figure 2.1 The basic steps of filtered back-projection reconstruction method. (a) Acquiring data projection. (b) Fourier Transform of the data. (c) Multiplication by frequency filter. (d) Inverse Fourier Transform of the data. (e) Back-projection of the filtered data (Rusinek, 1995).

2.1.1 Acquiring Data Projection

During image acquisition, a SPECT gamma camera rotates around a patient at various angles to create a series of planar images called projections as shown in Figure 2.2. A large number of projections must be acquired to adequately sample the field of view of the camera. For example in nuclear cardiology, it is generally accepted that adequate angular sampling can be achieved by collecting at least 30 uniformly spaced projection images over 180^{o} arc (1 projection every 6^{o}) (Germano, 2001).

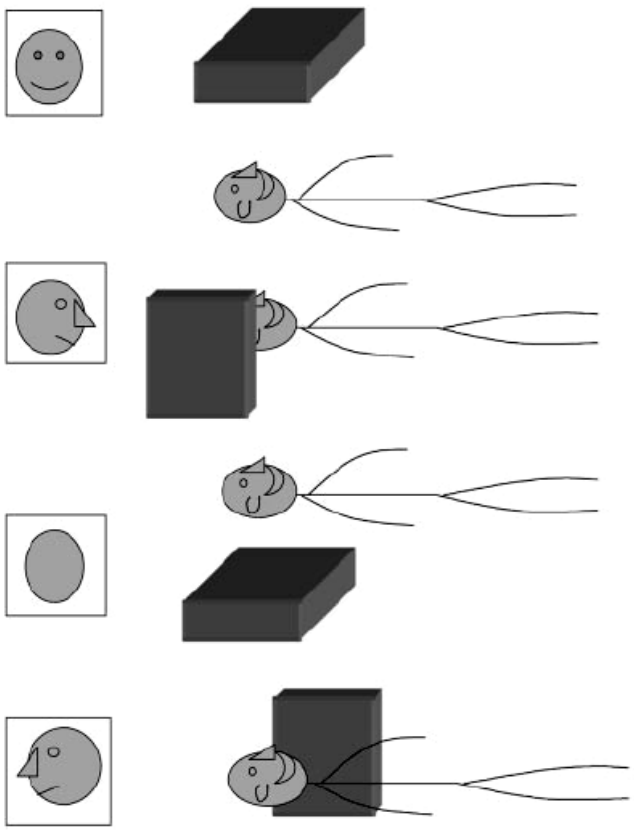

Figure 2.2 Projection data acquired from different views are used to reconstruct an image (Zeng, 2001).

In SPECT, collimator-detectors are used to acquire the projection data. At each stop of projection, only photons moving perpendicular to the camera face is assumed to pass through the collimator, called its line of response (Figure 2.3). The measured quantity sometimes is referred to as line integral for the line of response. A full set of line integrals recorded across the detector is called a projection, or a projection profile (Cherry *et al.*, 2003). As many of these photons originate from various depths in the patient, the result is an overlapping of all tracer emitting organs along the specific path, similar to what happened to an x-ray radiograph which is a superposition of all anatomical structures from three dimensions (3-D) into two dimensions (2-D).

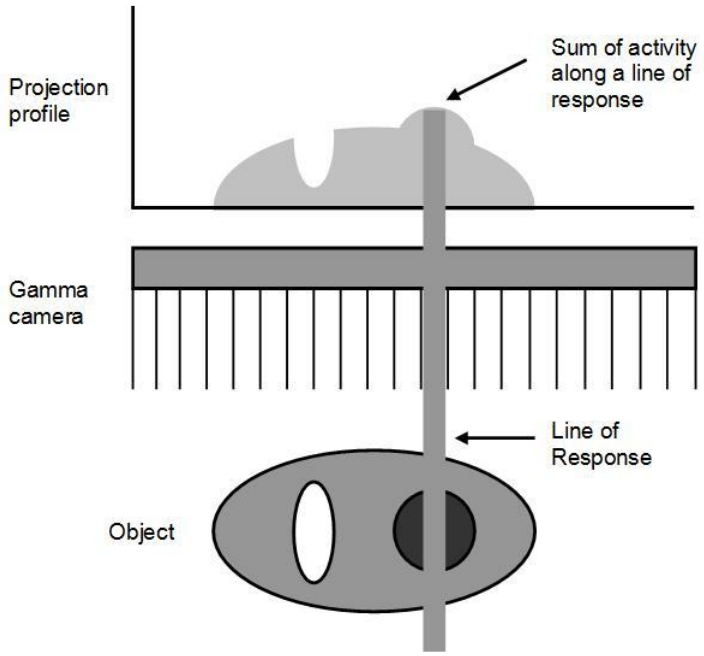

Figure 2.3 Cross section of the response characteristic of an idealized gamma camera. Each collimator hole views the radioactivity within a cylindrical perpendicular to the face of gamma camera, called its line of response. Under idealized conditions (such as no attenuation scatter) the signal recorded by the detector at that point reflects the sum of activity within the line of response. For a row of holes across the detector, the gamma camera generates a projection profile as shown. The projection profiles provide the data from which the image is reconstructed (Cherry *et al.*, 2003).

To determine how the radioactivity at a location (x, y) in the object contributes to the signal recorded in the projection profile, a new coordinate system (r, s) is introduced, which is stationary with respect to the gamma camera detector as illustrated in Figure 2.4 (Cherry *et al.*, 2003). If the camera is rotated by an angle ϕ with respect to the (x, y) coordinate system of the scanned object, the equations for transformation from (x, y) to (r, s) coordinates can be derived from the principle of similar triangles and given by

$$r = x\cos\phi + y\sin\phi \tag{2.1}$$

and

$$s = y\cos\phi - x\sin\phi \tag{2.2}$$

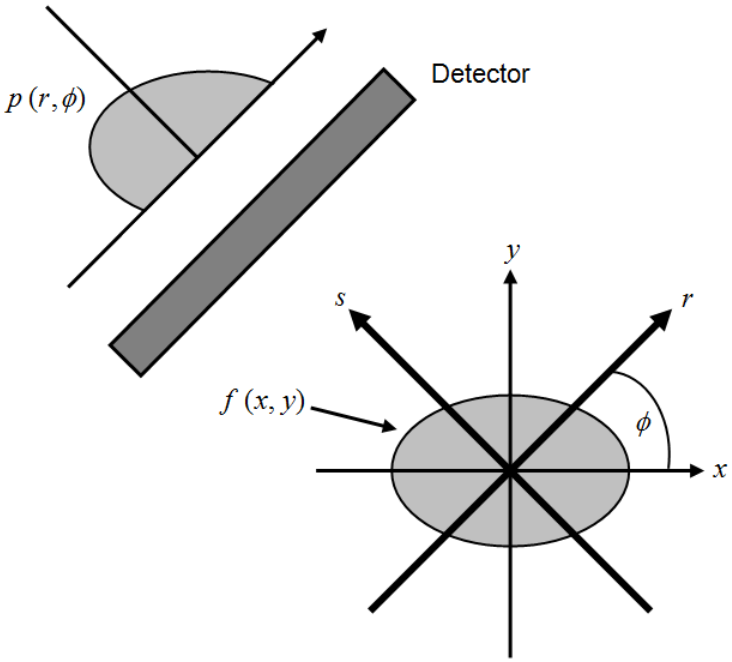

Figure 2.4 The (r, s) coordinate system is rotated by projection angle ϕ with respect to (x, y) coordinate system of the object and is fixed with respect to the gamma camera. The transformation $f(x,y)$ to $p(r,\phi)$ is actually based on Radon transform (Cherry *et al.*, 2003).

To display all the projection profiles for each slice, a sinogram is used as shown for a simple point-source object in Figure 2.5. It is a two dimension (2-D) of matrix $p(r,\phi)$, which each row across the matrix represents an intensity display across a single projection and the successive rows from top to bottom represent successive projection angles. The sinogram can be useful for determining the causes of artifacts in SPECT images (Cherry *et al.*, 2003).

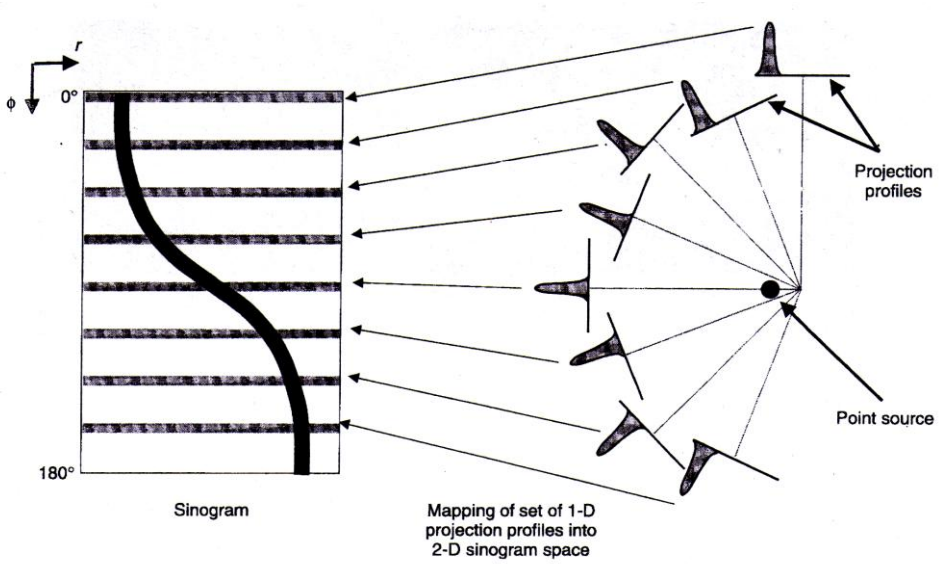

Figure 2.5 Two dimensional (2-D) intensity display of a set of projection profiles, known as sinogram. Each row in the display corresponds to an individual projection profile, sequentially displayed from top to bottom. A point source of radioactivity traces out of sinusoidal path in the sinogram (Cherry *et al.*, 2003).

2.1.2 Fourier Transform (FT) of Data

With the computer and fast Fourier Transform (FT) algorithm it is possible to shift from waveforms, or images, in the two-dimensional (2-D) case, to frequency spectra with enough speed and economy to create a new range of applications. Usually, FT can be calculated quickly and conveniently on personal computers, and many image and signal processing software packages contain FT routines (Cherry *et al.*, 2003).

In the reconstruction process particularly with FBP, the projection profiles provide the data from which the image is reconstructed. At that time, the data is in the form of spatial domain which the information on space refers to the counts corresponding to objects (organs, tumors) in the patient. For the purpose of filtering, the spatial information (in spatial domain) is converted to frequency information (in spatial frequency domain, also called k-space) by FT. The concept of spatial and frequency domain is illustrated in Figure 2.6. The data can also be filtered directly in the spatial domain using convolution, which is equivalent to a multiplication in the spatial frequency domain. However, it is a computationally intensive task to perform due to the quite complicated of mathematical description (Groch and Erwin, 2000).

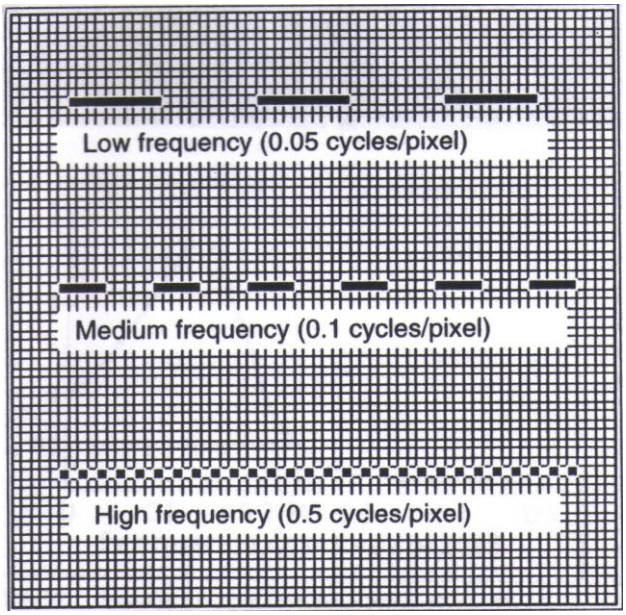

Figure 2.6 The intuitive way to visualize low, medium, and high frequencies in frequency domain. In spatial domain terms, one would say that the first object repeats itself every 20 pixels, the second every 10 pixels, and the third every 2 pixels. In frequency domain terms, one could equivalently say that the frequency of occurrence of the 3 objects is 0.05 times (or cycles) per pixel, 0.1 cycles per pixel, and 0.5 cycles per pixel, respectively (Germano, 2001).

Basically, SPECT image reconstruction relies on the projection slice theorem (or Fourier slice theorem). In words, this theorem says that the FT of the projection of a 2-D object along a projection angle ϕ (in other words, the FT of a 1-D profile, $p(r,\phi)$), is equal to the value of the 2-D FT of the object measured through the origin and along the same angle, ϕ, in k-space (note, the value of the FT, not the projection of the FT) as illustrated in Figure 2.7. Mathematically, the general expression for the projection slice theorem is

$$\mathcal{F}\left|p(r,\phi)\right| = F(k_r,\phi) \tag{2.3}$$

where $F(k_r,\phi)$ denotes the value of the FT measured at a radial distance k_r along a line at angle ϕ in k-space.

In FBP, the projection slice theorem is applied on the projection profiles in object space which are acquired at N projection angles, ϕ_i, i = 1, 2,…, N. Using the Equation 2.3, the 1-D FT of each profile is computed, which their values are then inserted at the appropriate coordinate locations in k-space. For a specific value of k_r in the FT of the projection acquired at a rotational angle ϕ, the data are inserted at rectangular coordinates given by

$$k'_x = k_r \cos\phi$$

$$k'_y = k_r \sin\phi \tag{2.4}$$

where primed notation is used to indicate that the coordinate locations do not correspond exactly to points on a rectangular grid. The inserted values are closely spaced near the origin and more widely spaced farther away from the origin, thus produce 1/r blurring or star artifact (where r is the distance from the center of the point-source location), which is a factor why the projection data is filtered before the back-projection (Cherry *et al.*, 2003).

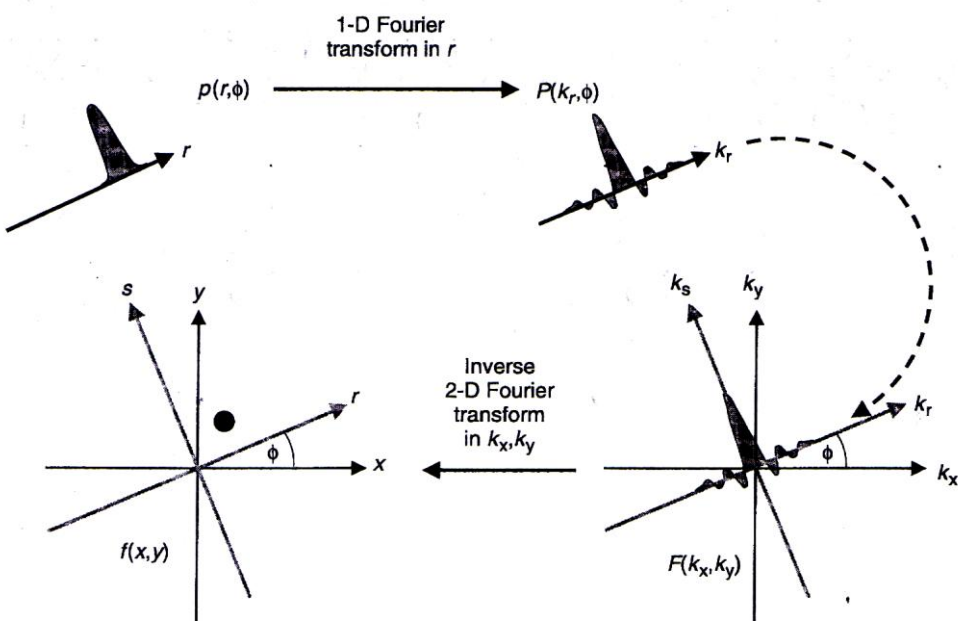

Figure 2.7 Concepts the projection slice theorem. $p(r,\phi)$ is a 1-D profile of the 2-D object $f(x,y)$ at projection angle ϕ. The theorem states that the 1-D Fourier Transform of this projection profile is equal to the values of the 2-D Fourier Transform of the object, $F(k_x,k_y)$, along a line through the origin of k-space at the same angle ϕ (Cherry *et al.*, 2003).

2.1.3 Data Filtering

The FT process produces 1/r blurring (star artifact) at the origin of k-space, where r is the distance from the center of the point-source location. In order to eliminate that blurring, a filter is applied to each k-space profile. Mathematically, this involves the multiplying each projection FT by Ramp filter which is denoted by $|k_r|$, the absolute value of the radial k-space coordinate at each point in the FT. The profile of a ramp filter is shown in Figure 2.8. The filtered FT for each projection is given by

$$P'(k_r,\phi) = |k_r| P(k_r,\phi) \tag{2.5}$$

where $P(k_r,\phi)$ is the unfiltered FT (Cherry *et al.*, 2003).

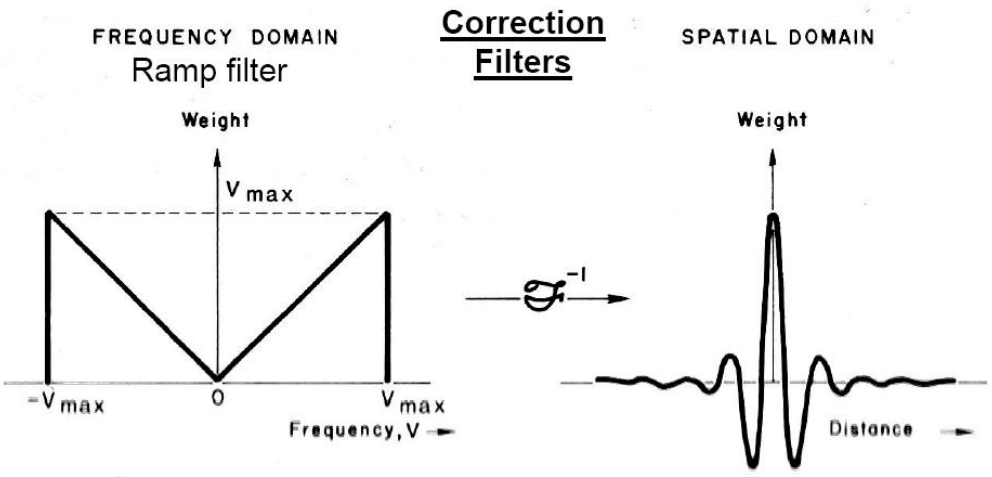

Figure 2.8 Ramp filter in frequency domain (left) and corresponding spatial domain filter (right). Ramp filter is Fourier Transform of spatial domain filter, which in turn is inverse Fourier Transform of Ramp filter (Germano, 2001).

Using Ramp filter to eliminate star artifact however has disadvantage, that is, since it amplifies the high frequency components of each projection, noise is also amplified and incorporated in the reconstructed image as illustrated in Figure 2.9 (A and B). Therefore, it is necessary to apply an additional window filter function (a noise smoothing filter), for example Butterworth filter in order to cut off the linear ramp around the point where the frequencies corresponding to the patient data disappear into the noise (Figure 2.9, C and D) (Groch and Erwin, 2000; Laere *et al.*, 2001; Powsner R.A. and Powsner E.R., 2006). The types of filters and their characteristics are explained in following section.

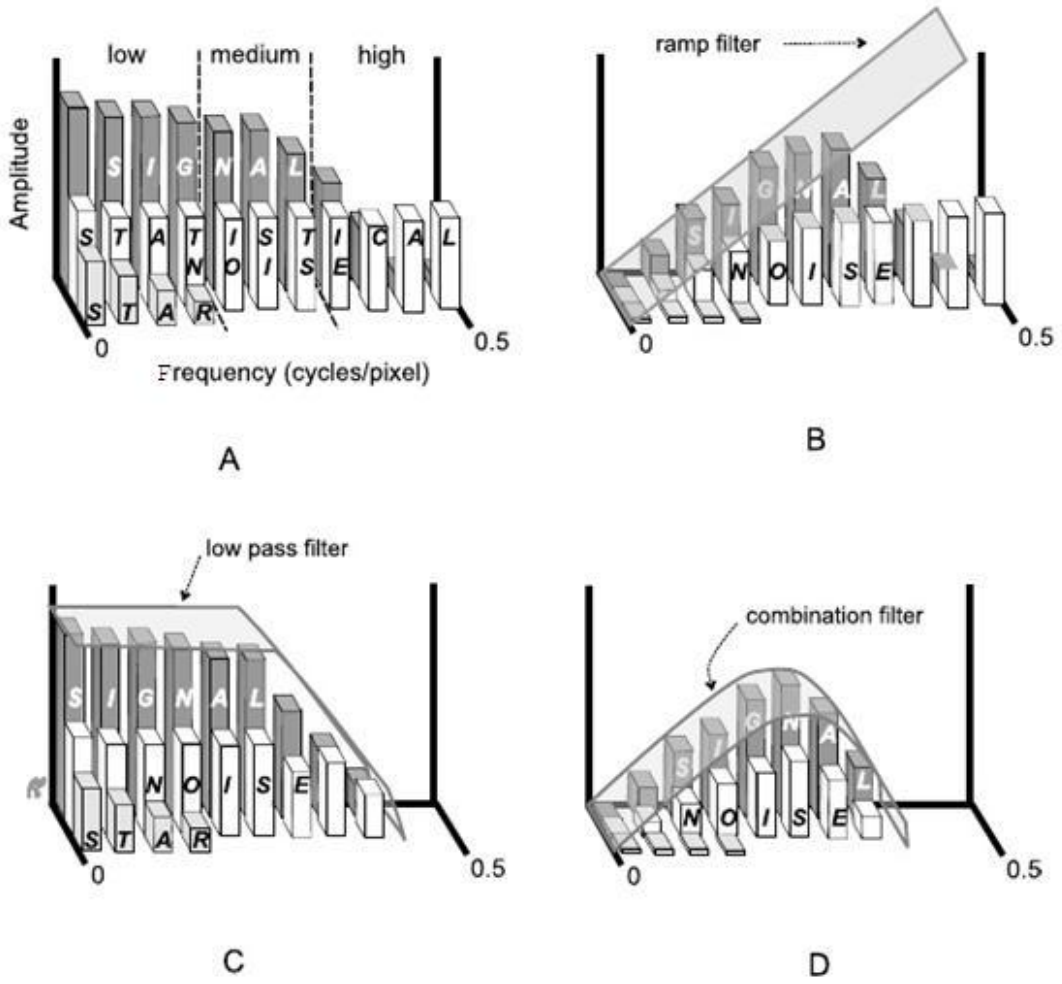

Figure 2.9 Effect of Ramp filter and additional low pass filters on signal data, statistical noise and the star artifact (Powsner R.A. and Powsner E.R., 2006).

2.1.4 Inverse Fourier Transform (FT) of Data

After the FT of each projection profile is filtered with Ramp and additional filter, it is then computed to obtain a projection profile in spatial domain using inverse FT. This is given by

$$\begin{aligned} p'(r,\phi) &= \mathcal{F}^{-1}\left[P'(k_r,\phi)\right] \\ &= F^{-1}\left[|k_r| P(k_r,\phi)\right] \end{aligned} \tag{2.6}$$

2.1.5 Back-Projection

Back-projection is the main reconstruction step of FBP. It involves the projecting (or distributing) of filtered projection profiles at their corresponding angle, ϕ, back through image matrix to obtain an approximation to the original object (Figure 2.10). The counts recorded in a particular projection profile element are divided uniformly amongst the pixels that fall within its projection path. Mathematically, the result is

$$f(x,y) = \frac{1}{N}\sum_{i=1}^{i=N} p'(x\cos\phi_i + y\sin\phi_i, \phi_i) \tag{2.7}$$

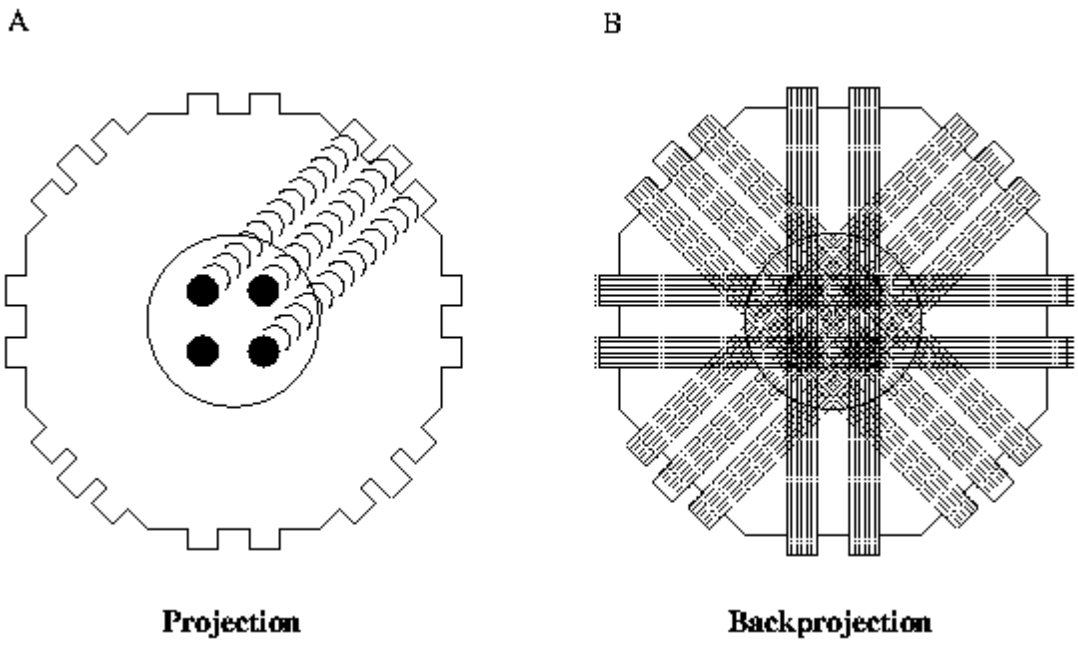

Figure 2.10 Illustration of projection (A) and back-projection (B).